

## Article

# A Highly Sensitive and Selective Near-Infrared Fluorescent Probe for Detecting Peroxynitrite in Living Cells and *Drosophila* Brains

Wei Wang, Jian-Bin Deng, Long Jin and Bai-Ou Guan \*

Guangdong Provincial Key Laboratory of Optical Fiber Sensing and Communication, Institute of Photonics Technology, Jinan University, Guangzhou 511443, China; wangwei\_0415@jnu.edu.cn (W.W.)

\* Correspondence: tguanbo@jnu.edu.cn; Tel.: +86-20-37337012

**Abstract:** Peroxynitrite ( $\text{ONOO}^-$ ) is a highly reactive nitrogen species (RNS) that is closely associated with many physiological and pathological processes. In this study, we construct a near-infrared (NIR) fluorescent probe, **NAF-BN**, that utilizes benzyl boronic acid ester for fluorescence quenching of naphthofluorescein cores. **NAF-BN** has been thoroughly evaluated for reliable imaging of exogenous  $\text{ONOO}^-$  in living cells. Further, **NAF-BN** can be applied effectively to visualize  $\text{ONOO}^-$  in *Drosophila* brains, confirming the hypothesis that neonicotinoid pesticides increase neurological damage and oxidative stress. The probe **NAF-BN** offers exciting potential to reveal the role of  $\text{ONOO}^-$  in various biological and medical fields.

**Keywords:** peroxynitrite; fluorescent probe; naphthofluorescein; cell imaging; *Drosophila*

## 1. Introduction

Peroxynitrite ( $\text{ONOO}^-$ ) represents a prominent reactive nitrogen species (RNS) in biological settings, engendered through the reaction of nitric oxide (NO) and superoxide radical anion ( $\text{O}_2^-$ ) in mitochondria and phagosomes [1–4]. Although this highly reactive specie is typically maintained at a relatively low steady-state concentration (nanomolar level) in vivo [5,6],  $\text{ONOO}^-$  is a potent endogenous oxidant and nitrating/nitrosating agent that is involved in signaling and redox regulation [7]. Its reactivity and ability to induce oxidative stress make it an important mediator of cellular damage and a contributing factor in various disease states. Furthermore,  $\text{ONOO}^-$  has been verified to have non-negligible implications for protein nitration/nitrosation, signaling pathway impairment, and immune cell dysfunction [8–12]. The distinctive characteristics of the modifications associated with the abnormal expression of  $\text{ONOO}^-$  have been identified as hallmarks of various diseases, such as inflammation [13–15], neurodegenerative diseases [16–18], cardiovascular diseases [19,20], liver injury [21,22], and even cancer [23]. The elucidation of the physiological mechanisms underlying the involvement of  $\text{ONOO}^-$  in various disease states is not yet fully determined due to the high reactivity, low concentration, and elusive in vivo reaction process of  $\text{ONOO}^-$ . Hence, it is essential to develop simple, efficient, and reliable methods to detect  $\text{ONOO}^-$  in various biological systems.

To date, several techniques have been developed for the detection of  $\text{ONOO}^-$  in biological systems, including electrochemical analysis [24,25], immunohistochemical analysis [26], and electron spin resonance spectroscopy [27]. However, some limitations of these techniques, such as complicated operation, time taken to complete, high instrument cost, and low spatial resolution, have promoted the exploration of alternative techniques. Fluorescence probe imaging has emerged as a promising alternative for the detection and visualization of trace targets. This technique offers superior spatial and temporal resolution, which makes it ideal for detecting trace amounts of  $\text{ONOO}^-$  in biological systems [28,29]. The design of a fluorescent probe for the detection of  $\text{ONOO}^-$  requires



**Citation:** Wang, W.; Deng, J.-B.; Jin, L.; Guan, B.-O. A Highly Sensitive and Selective Near-Infrared Fluorescent Probe for Detecting Peroxynitrite in Living Cells and *Drosophila* Brains. *Chemosensors* **2023**, *11*, 286. <https://doi.org/10.3390/chemosensors11050286>

Academic Editor: Young-Tae Chang

Received: 3 April 2023

Revised: 9 May 2023

Accepted: 9 May 2023

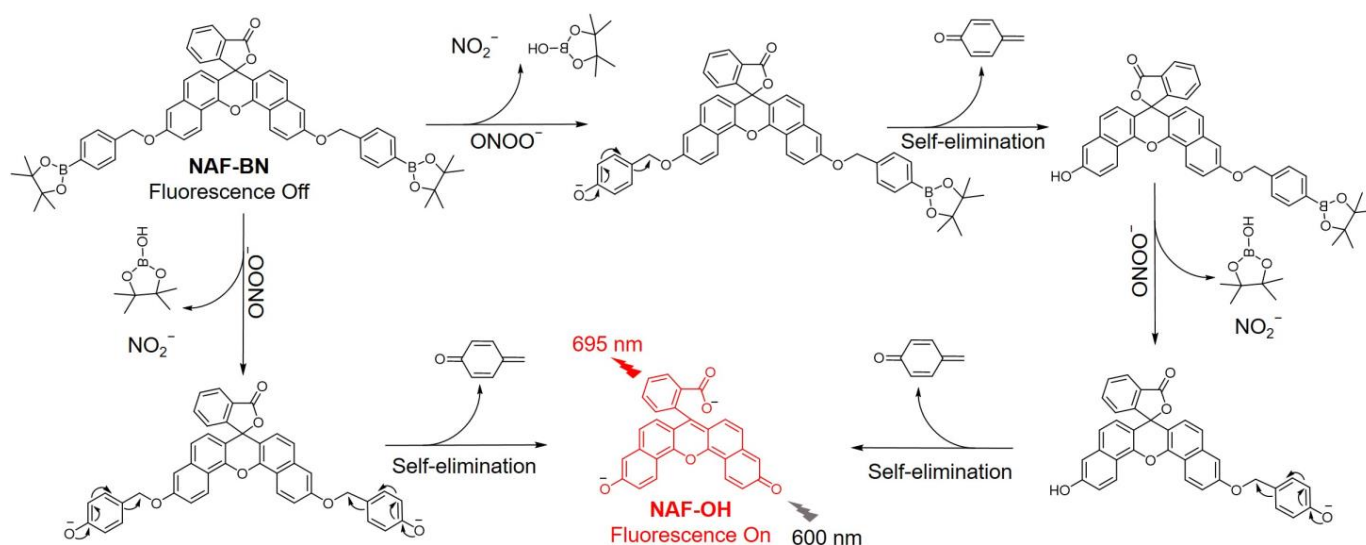
Published: 11 May 2023



**Copyright:** © 2023 by the authors. Licensee MDPI, Basel, Switzerland. This article is an open access article distributed under the terms and conditions of the Creative Commons Attribution (CC BY) license (<https://creativecommons.org/licenses/by/4.0/>).

a thorough understanding of the reactivity of  $\text{ONOO}^-$  and the specificity of the recognition group towards  $\text{ONOO}^-$ . Considering the strong oxidative and nucleophilic nature of  $\text{ONOO}^-$ , various fluorescent probes have been developed for the detection of  $\text{ONOO}^-$  based on different recognition groups, such as benzyl boronic acid groups [30–34],  $\alpha$  and  $\beta$ -unsaturated ketones [35–37], electron-rich phenolic groups [38–40], amides [41,42], olefins [43,44], diphenyl phosphoryl groups [45,46], etc. Moreover, the well-known high background autofluorescence of endogenous biomolecules can interfere with the detection and imaging of the fluorescent probe. In consequence, near-infrared (NIR) fluorescent probes with improved imaging capabilities that can penetrate deeper into tissues and reduce background autofluorescence have gained widespread attention. Among the various probes, cyanine (Cy) derivatives have been frequently utilized due to their superior optical properties, such as high quantum yields, excellent photostability, and good solubility in aqueous environments [47–54]. To optimize the NIR fluorescent performance of Cy-based probes, a commonly employed strategy is to incorporate critical structural components such as recognized electron-donating groups, cationic receptors, and carbon–carbon double bond linkers into the probe molecule. However, the strong electro-pulling ability of the cationic receptor (such as indole group) in a Cy-based probe can lead to the formation of highly reactive methylene and double bond sites. Double bonds are susceptible to nucleophilic addition by reactive sulfur species ( $\text{HS}$ ,  $\text{SO}_3^{2-}$ ) [55], and methylene sites are prone to oxidative decomposition by ROS/RNS ( $\text{ONOO}^-$ ,  $\text{H}_2\text{O}_2$ ) [56]. Alterations in the molecular structure of probes can seriously affect fluorescence detection and may also produce undesirable drug efficacy and other side effects. Hence, the design of fluorescent probe molecules that possess a rational structure is of utmost importance. In summary, the high reactivity and complexity of the *in vivo* detection environment, as well as the low  $\text{ONOO}^-$  expression, require  $\text{ONOO}^-$  fluorescent probes with excellent NIR fluorescence sensitivity, selectivity, and chemical stability.

Boronates are emerging as one of the most effective identification groups for detecting and quantifying hydrogen peroxide and peroxyxynitrite and were often used to develop hydrogen peroxide and peroxyxynitrite fluorescent probes previously [30–34,57–62]. Herein, we present a NIR fluorescent probe for  $\text{ONOO}^-$  detection, namely **NAF-BN**, that is based on a naphthalene fluorescein scaffold and contains a benzyl boronic acid ester recognition group. The naphthalene fluorophores of the probe have a polycyclic conjugated structure, which provides excellent NIR fluorescence quantum yields and chemical stability. The boronic ester moiety was chosen over the boronic acid in an attempt to increase lipophilicity and therefore cell permeability [63]. In addition, boronic ester–benzyl ether linkage indicated superior aqueous stability [62] and substituted phenylboronates have a greater reaction rate constant for peroxyxynitrite than aliphatic boronates at pH 7.4 [64]. The sensing mechanism of the probe involves  $\text{ONOO}^-$ -induced oxidation and hydrolysis of the boronic acid ester (Scheme 1), which triggers the isomerization of the lactone spiro ring of the probe and results in a fluorescence “off-on” effect with short response times. **NAF-BN** has been successfully used to visualize  $\text{ONOO}^-$  levels in living cells. Additionally, **NAF-BN** has exhibited potential in verifying the hypothesis that the neonicotinoid pesticide imidacloprid induces brain neural damage and increases oxidative stress in a *Drosophila* model.



**Scheme 1.** The sensing mechanism of NAF-BN.

## 2. Materials and Methods

### 2.1. Spectral Characterization of the Probe

Stock solutions (2 mM) of **NAF-BN** and **NAF-OH** were prepared by dissolving them in DMSO. Test samples were prepared by mixing 10  $\mu$ L of the **NAF-BN** stock solution with the desired volume of the analyte in a 5 mL centrifuge tube. The volume of the test sample solution was then adjusted to 4 mL with phosphate buffer (100 mM PB, pH 7.4, containing 50% DMSO) and the mixture was incubated at room temperature for a specified time period. Subsequently, the solution was transferred to a quartz cuvette and the absorption and fluorescence spectra were recorded separately. The fluorescence excitation wavelength was set at 600 nm with an emission wavelength range of 620 to 900 nm. The limit of detection was calculated based on  $LOD = 3\sigma/k$ , where  $\sigma$  is the standard deviation of the blank measurement and  $k$  is the slope of the fluorescence intensity versus the ONOO<sup>-</sup> concentration.

The fluorescence quantum yield is calculated according to the equation:

$$Q = Q_R \frac{I}{I_R} \frac{A_R}{A} \frac{n^2}{n_R^2}$$

$Q$  is the quantum yield,  $I$  is the integrated intensity,  $n$  is the refractive index, and  $A$  is the optical density. The subscript  $R$  is the reference fluorophore with a known quantum yield.

### 2.2. Cytotoxicity Assay

For cytotoxicity assay, the viabilities of mouse breast cancer cells (4T1 cells) and human normal liver cells (HL-7702 cells) were assessed using the CCK-8 assay. 4T1 cells and HL-7702 cells were purchased from iCell Bioscience Inc. (Shanghai, China) and maintained in a 37  $^{\circ}$ C, 5% CO<sub>2</sub> environment. **NAF-BN** was dissolved in DMSO with a final DMSO content of less than 1%. The cells were divided into three replicate groups and treated with 0.001, 0.01, 0.1, 1, 10, 30, and 50  $\mu$ M **NAF-BN** or **NAF-OH**. A control group of untreated cells was maintained in an equal volume of medium. In addition, the cell viabilities of HL-7702 and 4T1 cells incubated with **NAF-BN** and 3-morpholinosydnonimine hydrochloride (SIN-1) or **NAF-BN** and phorbol-12-myristate 13-acetate (PMA)/lipopolysaccharide (LPS) were also determined. After 24 h of incubation, the cells were washed three times with PBS, 10% CCK-8 was added, and the mixture was incubated in a 37  $^{\circ}$ C, 5% CO<sub>2</sub> environment for 2 h. The absorbance was measured at 450 nm using an enzyme marker.

### 2.3. Fluorescence Imaging of HeLa Cells

HeLa cells were purchased from iCell Bioscience Inc. and incubated in DMEM supplemented with 10% FBS at 37 °C with 7.5% CO<sub>2</sub>. Before the experiment,  $1 \times 10^5$  HeLa cells were inoculated into confocal culture dishes and incubated in a 37 °C incubator for 24 h.

SIN-1, a well-known generator for ONOO<sup>-</sup>, was used to provide exogenous ONOO<sup>-</sup>, and the ONOO<sup>-</sup> was removed by minocycline [65,66]. Phorbol-12-myristate 13-acetate (PMA) and lipopolysaccharide (LPS) was used to stimulate endogenous ONOO<sup>-</sup> production in cells. It has been demonstrated that PMA can activate potential NADPH oxidase (NOX) to produce O<sub>2</sub><sup>-</sup> and LPS can stimulate NO synthase (iNOS) to produce NO, which together induce the overexpression of ONOO<sup>-</sup> [67,68]. The experimental methods and procedures refer to the studies [33,47,48,56,69–74]. The probes are prepared with DMSO as a 5 mM stock solution and then diluted to 10 μM using cell culture medium (DMSO = 0.2%). Each time the medium is changed, the medium from the previous step is cleaned up. Four groups of cells were prepared for imaging using NAF-BN (10 μM). The first group was incubated with NAF-BN (10 μM) for 30 min, rinsed with PBS three times, and imaged. The second group was pretreated with NAF-BN (10 μM) for 30 min, then incubated with SIN-1 (100 μM, peroxyxynitrite donor) for 1 h, rinsed three times with PBS, and imaged. The third group was pretreated with NAF-BN (10 μM) and minocycline (100 μM; ROS scavenger) for 30 min, then incubated with SIN-1 (100 μM) for 1 h, washed three times with PBS, and imaged. The fourth group was incubated with NAF-BN (10 μM) for 30 min, then incubated with PMA (50 μM) and LPS (50 μM) for 4 h, washed three times with PBS, and imaged. In addition, cell nuclei were stained with DAPI for 30 min, washed with PBS, and imaged. Confocal shooting: DAPI was acquired using an excitation wavelength of 405 nm and an emission wavelength range of 410–450 nm (blue channel). Probe fluorescence imaging was acquired using an excitation wavelength of 600 nm and an emission wavelength of 690 nm (red channel).

### 2.4. Fluorescence Imaging of Drosophila Brains

Wild-type *Drosophila* (w1118) was purchased from TsingHua Fly Center. *Drosophila* were fed with corn flour syrup medium and bred at room temperature. The experimental procedure from [75] was adopted. The experiments were divided into three groups, each containing three brains. In the first group, *Drosophila* brains were treated with NAF-BN (50 μM) for 30 min, then washed with PBS and imaged. In the second group, *Drosophila* brains were first treated with SIN-1 (3 mM) for 4 h, then exposed to NAF-BN (50 μM) for 30 min and finally cleaned with PBS for imaging. In the third group, *Drosophila* was treated with imidacloprid (10 ppm), and the isolated *Drosophila* brains were incubated with NAF-BN (50 μM) for 30 min, then washed with PBS and imaged.

Imidacloprid was prepared as a 1000 ppm solution in DMSO and was further diluted to 10 ppm with 5% sucrose solution for exposure experiments. DMSO was substituted for imidacloprid and added to 5% sucrose solution as a control. Fluorescence imaging was performed using a fluorescent stereomicroscope (Mshot, MZX81, Guangzhou, China) equipped with an Olympus 1× flat-field compound achromatic objective. The excitation wavelength range used was 590–650 nm, with a 660 nm filter, and the collection wavelength range was 663–737 nm.

## 3. Results and Discussion

### 3.1. Design and Synthesis

Naphthofluorescein is a highly efficient NIR fluorescent backbone that has been used in the design of various fluorescent probes due to its chemical stability, facile modification, NIR emission, and superior biocompatibility [76]. Among several naphthalene fluorescein skeletons (Figure S1), NAF-OH, with the advantages of NIR emission and chemical stability, was chosen as the fundamental backbone, whereas structures 1, 2, and 3 produce shorter emission wavelengths [77,78]. In addition, another notable factor is that NAF-OH comprises a phenolic hydroxyl structure with a pK<sub>a</sub> of  $7.99 \pm 0.02$  in the physiological pH range,

which facilitates the opening of the lactone spiro ring to emit fluorescence. In contrast, structures 4 and 5 have higher  $pK_a$  values [76], are ketones in the physiological pH range, and cannot provide electrons to generate a fluorescence effect. The benzyl boronic acid ester was built as the recognition group to shield the **NAF-OH** naphthol, providing a lactone spirocyclic closed structure to quench the fluorescence. The presence of a carboxyl group with a spironolactone structure (closed-loop state) could result in the whole molecular backbone structure of the probe adopting a non-conjugated structure, with no absorption or fluorescence. Once interacted with  $ONOO^-$ , the boronic ester, as recognition module of **NAF-BN**, would be oxidized. A subsequent secondary hydrolysis reaction leads to the production of tertiary alcohols, which facilitate the departure of protecting groups and the formation of naphthol structure **NAF-OH**. Such a structural transformation triggers the opening of the lactone spiro ring to form carboxylates by electron redistribution and fluorescence release. The sensing mechanism of **NAF-BN** has been demonstrated by MS in Figure S2, a peak for **NAF-OH** was found in the mass spectrum of **NAF-BN** after reaction with  $ONOO^-$ . The specific synthetic route of **NAF-BN** and the details of the materials and instruments used in this study are provided in the supplementary materials.

### 3.2. Sensing Abilities of **NAF-BN**

The optical response of the probe **NAF-BN** to  $ONOO^-$  in phosphate buffer was confirmed by UV-vis and fluorescence spectroscopies. Prior to treatment with  $ONOO^-$ , no absorption could be observed with only **NAF-BN**. However, upon in the presence of  $100 \mu\text{M } ONOO^-$ , a distinct absorption band emerged, with an absorption peak at 620 nm (Figure 1a). Whereas **NAF-BN** demonstrated negligible fluorescence emission initially, the addition of  $100 \mu\text{M } ONOO^-$  resulted in a remarkable 50-fold fluorescence enhancement at 695 nm (Figure 1b). The absorption and emission spectra of **NAF-OH** overlap with the absorption and emission spectra of **NAF-BN** +  $ONOO^-$ , this could prove that the fluorescence produced after the reaction is attributed to the release of **NAF-OH** (Figure S3). The quantum yield in the fluorescence-on state is 0.125, whereas in the fluorescence-off state it is 0.0026. The observed increase in fluorescence intensity is believed to be a consequence of the  $ONOO^-$ -mediated opening of the naphthofluorescein ring structure. The naphthol group present in **NAF-OH** is highly susceptible to protonation and deprotonation at different pH levels, which may alter fluorescence behavior of the probe. Therefore, we verified the response of **NAF-BN** to  $ONOO^-$  at different pH levels (Figure S4). The results showed that  $ONOO^-$ -induced fluorescence turn-on behavior was minimally affected in neutral and weakly alkaline environments, whereas low pH values resulted in fluorescence quenching. The fluorescence intensity is highly sensitive to even small changes in pH; this will be a potential limitation of the probe. As presented in Figure S5, the fluorescence response of **NAF-BN** at different pH values is mainly attributed to the protonation state of **NAF-OH**. In alkaline environments, **NAF-OH** is a ketone and the lactone opens the ring, releasing fluorescence. To replicate the in vivo detection environment, the physiological pH (pH = 7.4) was chosen as the working pH for subsequent experiments.

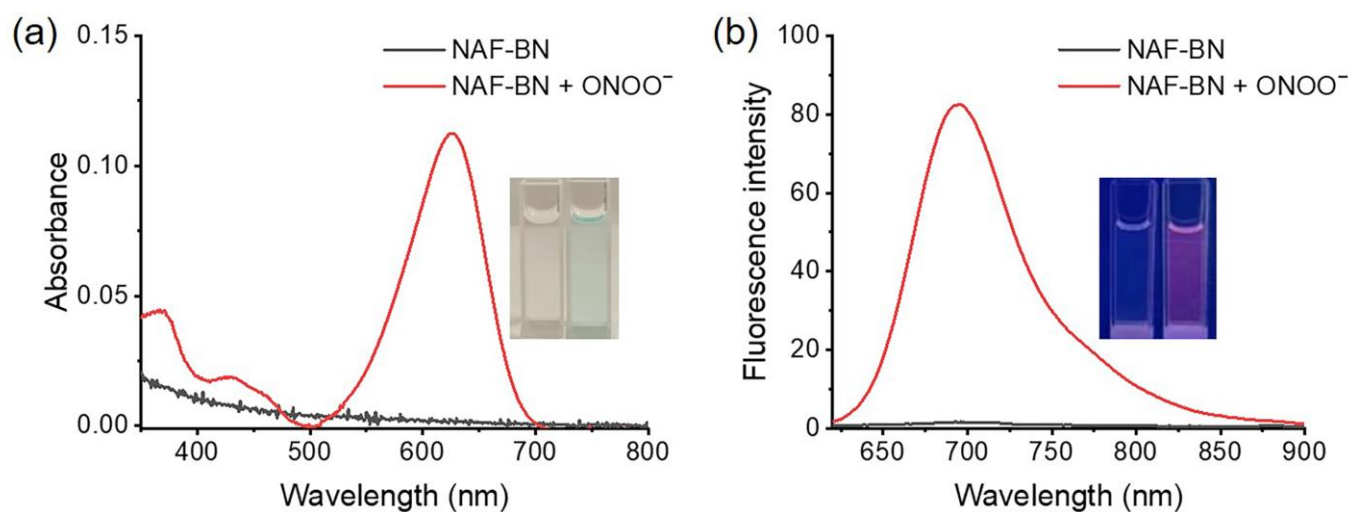


**Figure 1.** Absorption (a) and fluorescence spectra (b) of **NAF-BN** (5  $\mu$ M) before (black line) or after (red line) reaction with  $\text{ONOO}^-$  (100  $\mu$ M) for 15 min in phosphate buffer (100 mM PB, pH 7.4, with 50% of DMSO).  $\lambda_{\text{ex}}$  = 600 nm; slits = 5 nm/5 nm. Inset: change in solution before and after the reaction of the **NAF-BN** with  $\text{ONOO}^-$  under daylight or UV lamp (365 nm).

In biological systems,  $\text{ONOO}^-$  reacts rapidly with bio-reductive substances such as thiol-containing molecules or proteins. Thus, it is essential that the probe used to detect  $\text{ONOO}^-$  presents a fast response time to track such dynamic changes. To evaluate the response time of **NAF-BN**, the probe was reacted with varying concentrations of  $\text{ONOO}^-$ . As illustrated in Figure 2a, **NAF-BN** exhibited an obvious fluorescence response to all three different concentrations of  $\text{ONOO}^-$ . The fluorescence signal reached a maximum and stabilized within 100 s after the addition of 100  $\mu$ M  $\text{ONOO}^-$ . Notably, even at lower concentrations (20  $\mu$ M) of  $\text{ONOO}^-$  the reaction equilibration could be reached in a relatively fast time (5 min). As the lifetime of  $\text{ONOO}^-$  under the conditions used is  $<1$  s, the delayed formation of the fluorescence intensity must be due to the dynamics of the release of the quinone product from the primary phenolic product of **NAF-OH**. These results indicate that **NAF-BN** exhibits a short response time (within 100 s) to  $\text{ONOO}^-$  and can potentially be used to detect  $\text{ONOO}^-$  in biological systems.

The sensitivity and quantitative detection ability of a probe are crucial factors for its utility in biological systems. Therefore, in this study we investigated the sensitivity of **NAF-BN** to  $\text{ONOO}^-$  through titration experiments. As shown in the figure (Figure 2b), the fluorescence emission gradually increased with the increasing concentrations of  $\text{ONOO}^-$ . A linear relationship was observed between the concentrations of  $\text{ONOO}^-$  and the fluorescence emission intensity at 695 nm in the range of 0–5  $\mu$ M, indicating that **NAF-BN** can achieve effective detection of  $\text{ONOO}^-$  in this concentration range (Figure 2c). The calculated limit of detection (LOD) of the probe **NAF-BN** was found to be 436 nM, which is in the physiological concentration range of  $\text{ONOO}^-$  [6]. This implies that the probe can potentially be used to monitor endogenous  $\text{ONOO}^-$  levels in biological systems.

In order to eliminate the interference of common ROS/RNS and thiols in detection for  $\text{ONOO}^-$ , the selectivity of **NAF-BN** towards  $\text{ONOO}^-$  is particularly important. As depicted in Figure 2d, the fluorescence signal of the probe remains negligible and does not interfere with  $\text{ONOO}^-$  detection even if the interferer concentration is 10 times higher than that for  $\text{ONOO}^-$ , except for  $\text{H}_2\text{O}_2$ . We also re-tested the selectivity of **NAF-BN** in acetonitrile and 1,4 dioxane with generally similar results (Figure S9). It is noteworthy that the reaction of  $\text{H}_2\text{O}_2$  and boronates has been reported; however, the reaction rate of  $\text{H}_2\text{O}_2$  to boronates is much slower than that of  $\text{ONOO}^-$ , with a difference of several orders of magnitude between their reaction rates [64], which is consistent with our experimental results (Figure S7). This finding suggests that **NAF-BN** is selective towards  $\text{ONOO}^-$  and exhibits no significant interference from  $\text{H}_2\text{O}_2$  during short incubation times (15 min) at

pH 7.4. We further investigated the effect of pH on the selectivity of **NAF-BN** towards the detection of  $\text{ONOO}^-$ . At pH = 9,  $\text{H}_2\text{O}_2$  interfered with the detection of  $\text{ONOO}^-$  due to accelerated reaction kinetics (Figure S8). Overall, **NAF-BN** has excellent chemical stability, near-zero fluorescence background, a 200 s response time, and good selectivity at pH 7.4, meaning it has the potential for  $\text{ONOO}^-$  fluorescence imaging of live cells and organisms.

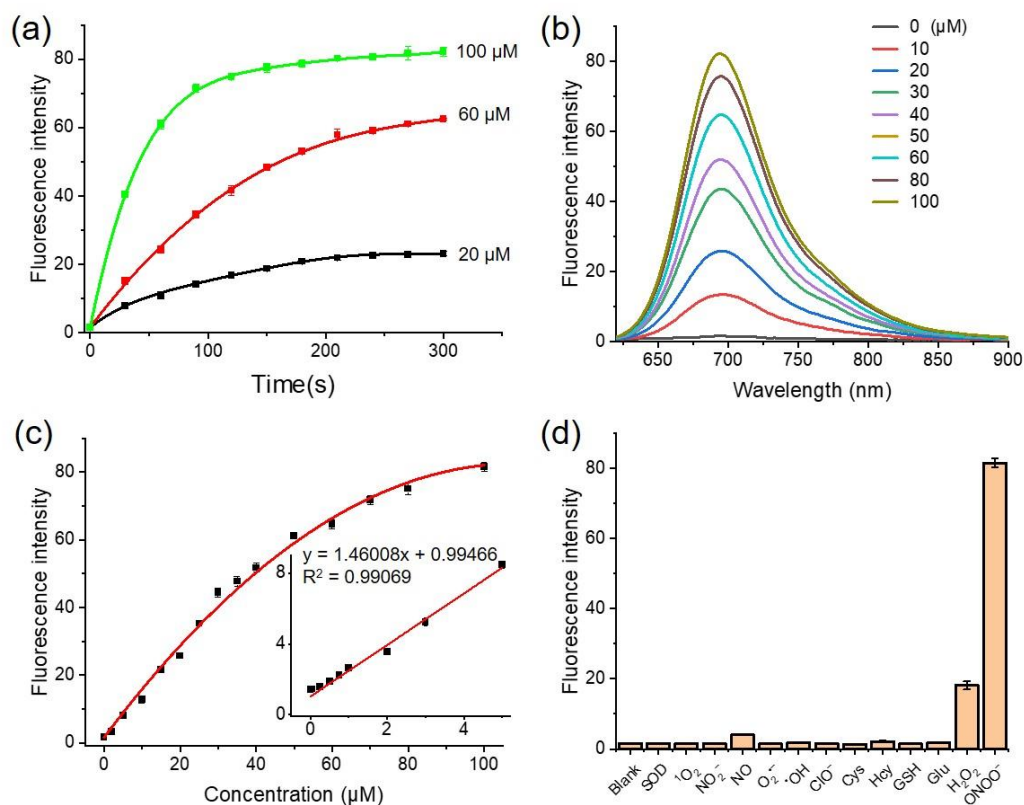


**Figure 2.** (a) Time-dependent fluorescence intensity of **NAF-BN** at 695 nm in the presence of different concentrations of  $\text{ONOO}^-$ . (b) The changes in the fluorescence spectra of **NAF-BN** upon the addition of different concentrations of  $\text{ONOO}^-$  for 15 min. (c) Fluorescence intensity changes of **NAF-BN** (5  $\mu\text{M}$ ) at 695 nm as a function of the concentrations of  $\text{ONOO}^-$  (0–100  $\mu\text{M}$ ). The fluorescence intensity changes as a function of the low concentration of  $\text{ONOO}^-$  from 0 to 5  $\mu\text{M}$  and was linearly fitted (inset). (d) Fluorescence response to **NAF-BN** and different analytes for 15 min:  $\text{ClO}^-$ ,  $^1\text{O}_2$ ,  $\text{NO}_2^-$ , NO,  $\text{O}_2^-$ , OH, Cys, Hcy, GSH, glucose,  $\text{H}_2\text{O}_2$  (1 mM);  $\text{ONOO}^-$  (100  $\mu\text{M}$ ); and SOD (50 U/mL). All experiments were performed in phosphate buffer (100 mM PB, pH 7.4, with 50% DMSO), the concentration of **NAF-BN** was 5  $\mu\text{M}$ ;  $\lambda_{\text{ex}} = 600$  nm; slits = 5 nm/5 nm.

### 3.3. Bioimaging of $\text{ONOO}^-$ in HeLa Cells

Prior to imaging live cells, it is crucial to verify the toxicity of the probe to ensure its biocompatibility. Here, we performed a CCK-8 assay to evaluate the cytotoxicity of **NAF-BN** towards mouse breast cancer cells (4T1 cells) and human normal liver cells (HL-7702 cells). The cells were treated with various concentrations of **NAF-BN** and **NAF-OH** for 24 h and then cell viability was assessed. As illustrated in Figure 3a and Figure S10, even at 50  $\mu\text{M}$  **NAF-BN** showed low cytotoxicity towards the cells. Incubation with **NAF-BN** + SIN-1 had little effect on cell viability (Figure S12), whereas cells incubated with **NAF-BN** + PMA/LPS retained over 60% cell viability after 24 h, demonstrating that this sensing reaction may have some cytotoxicity potential. However, as shown in Figure S11, a significant decrease in cell viability occurred at **NAF-OH** concentrations above 10  $\mu\text{M}$ , whereas concentrations below 0.01  $\mu\text{M}$  are safe for cells.

Here, we performed a fluorescence imaging experiment in HeLa cells to investigate the imaging ability of **NAF-BN** for both exogenous and endogenous  $\text{ONOO}^-$  (Figure 3b).

Almost no fluorescence was observed in cells incubated with only 10  $\mu\text{M}$  **NAF-BN**, suggesting low levels of  $\text{ONOO}^-$  in HeLa cells. We then stimulated the production of  $\text{ONOO}^-$  by treating the cells with 100  $\mu\text{M}$  SIN-1, a generator of  $\text{ONOO}^-$ . The fluorescence signal was significantly enhanced, suggesting that **NAF-BN** is capable of detecting exogenous  $\text{ONOO}^-$ . To verify the specificity of **NAF-BN** for  $\text{ONOO}^-$ , we treated the cells with SIN-1 followed by 100  $\mu\text{M}$  minocycline ( $\text{ONOO}^-$  cleavage agent). As expected, the results showed that the fluorescence signal was weakened, indicating that  $\text{ONOO}^-$  was cleared successfully and that the fluorescence signal indeed originated from  $\text{ONOO}^-$ . In the following, we aimed to stimulate endogenous  $\text{ONOO}^-$  production in HeLa cells and observed it with **NAF-BN**. We used PMA and LPS to co-treat the cells and observed a significant fluorescence signal, supporting the ability of **NAF-BN** to detect oxidative stress in cells. In vitro experiments have demonstrated that **NAF-BN** also responds to hydrogen peroxide. Therefore the fluorescence emission may also originate from hydrogen peroxide produced by the cells. However, the probe reacts faster with peroxynitrite than hydrogen peroxide under the same conditions, so the fluorescence emission is mainly attributable to the oxidation of the probe by peroxynitrite. Quantitative statistics showed that the average fluorescence of cells treated with SIN-1 or PMA/LPS was enhanced by 10.3-fold and 10.9-fold, respectively, compared with untreated cells (Figure 3c). In summary, **NAF-BN** has good biocompatibility as well as excellent imaging ability for exogenous and endogenous cellular  $\text{ONOO}^-$ .

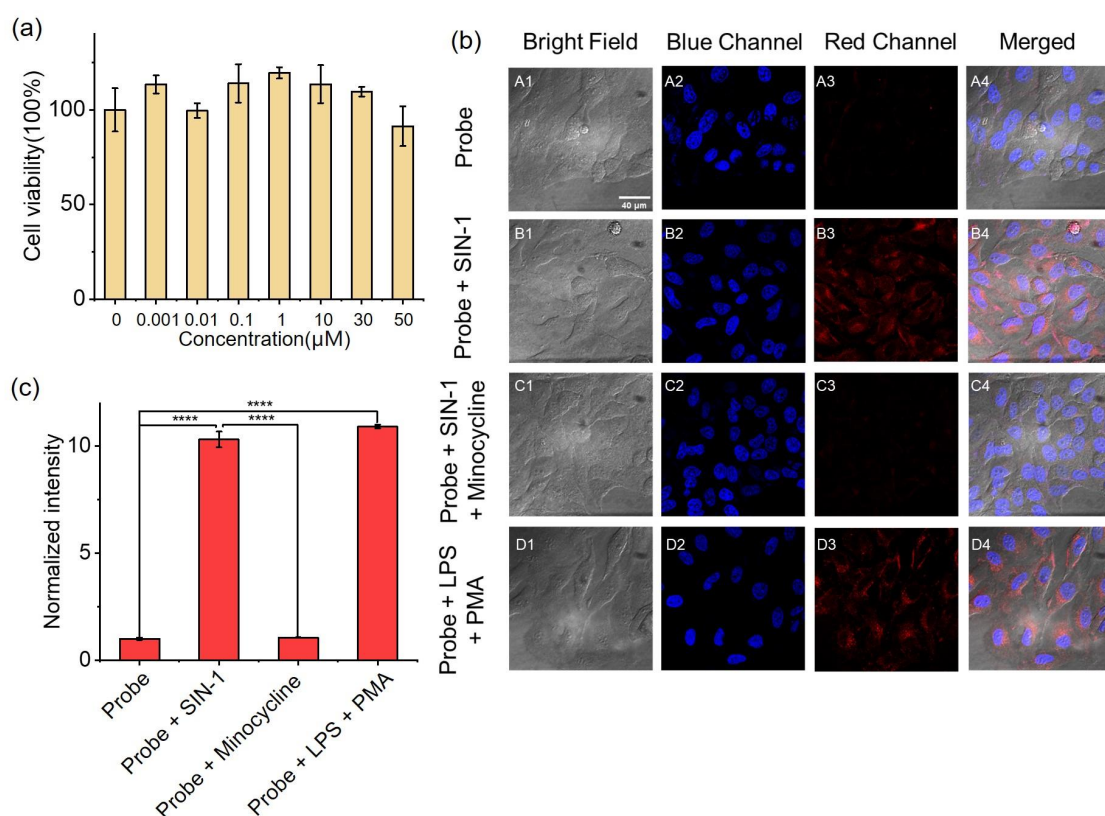


**Figure 3.** (a) Cell viability of HL-7702 cells incubated with different concentrations of **NAF-BN**, as assessed by CCK-8 assays (incubation time 24 h). (b) Fluorescence imaging of HeLa cells: (A1–A4) the cells incubated with **NAF-BN** for 30 min; (B1–B4) the cells incubated with **NAF-BN** for 30 min followed by the addition of SIN-1 (100  $\mu\text{M}$ ) for another 1 h; (C1–C4) the cells incubated with **NAF-BN** and minocycline (100  $\mu\text{M}$ ; ROS scavenger) for 30 min, followed by incubation with SIN-1 (100  $\mu\text{M}$ ) for 1 h; (D1–D4) the cells incubated with **NAF-BN** for 30 min, then treated with PMA (50  $\mu\text{M}$ ) and LPS (50  $\mu\text{M}$ ) for 4 h; blue channel: DAPI staining. All experiments were performed with 10  $\mu\text{M}$  **NAF-BN**. The scale bar is 40  $\mu\text{m}$ . (c) The histogram represents the mean fluorescence intensities of the corresponding cells. \*\*\*\* Indicates a significant difference ( $p < 0.0001$ ),  $n = 4$ .

### 3.4. Bioimaging of ONOO<sup>-</sup> in *Drosophila* Brains

The imaging ability of NAF-BN for detection of ONOO<sup>-</sup> in an actual animal model was further evaluated. The small size, ease of handling, and quick reproductive rate of *Drosophila* make it a highly suitable model organism for the study of human diseases [79]. Imidacloprid is a neonicotinoid insecticide that acts as an agonist of insect nicotinic acetylcholine receptors (nAChRs) and negatively affects neurotransmission. Imidacloprid has been confirmed to induce increased neurological damage and oxidative stress in the insect brain [80,81]. Thus, NAF-BN was used to verify the possibility of pesticide-induced oxidative stress in *Drosophila* brains. The fluorescence imaging results are presented in Figure 4a. The brains of *Drosophila* treated with only NAF-BN showed no fluorescence signal. Conversely, the brains treated with 3 mM SIN-1 and NAF-BN exhibited red fluorescence, demonstrating that the normal *Drosophila* brain has low expression of endogenous ONOO<sup>-</sup>. Next, we treated *Drosophila* with 10 ppm imidacloprid; a clear red fluorescence could be observed, confirming the production of endogenous ONOO<sup>-</sup> or H<sub>2</sub>O<sub>2</sub>. Since NAF-BN reacts much more slowly with hydrogen peroxide than peroxyntirite at pH 7.4 under the same conditions, we consider that the fluorescence emission is mainly attributed to peroxyntirite. These findings suggest that ONOO<sup>-</sup> may originate from imidacloprid-induced oxidative stress. The binding sites of *Drosophila* nicotinic acetylcholine receptors (nAChRs) exposed to low doses of imidacloprid are occupied by imidacloprid, resulting in a continuous opening of Ca<sup>2+</sup>, K<sup>+</sup>, and Na<sup>+</sup> cation channels, a continuous influx of cations into neurons, and increased oxidative stress [82]. Our statistical quantification of the above images yielded that the average fluorescence of brains treated with SIN-1 or imidacloprid was signally enhanced (Figure 4b). The fluorescence imaging experiments with HeLa cells and *Drosophila* brains highlight the potential of NAF-BN as a powerful tool for the detection of ONOO<sup>-</sup> levels in organisms.

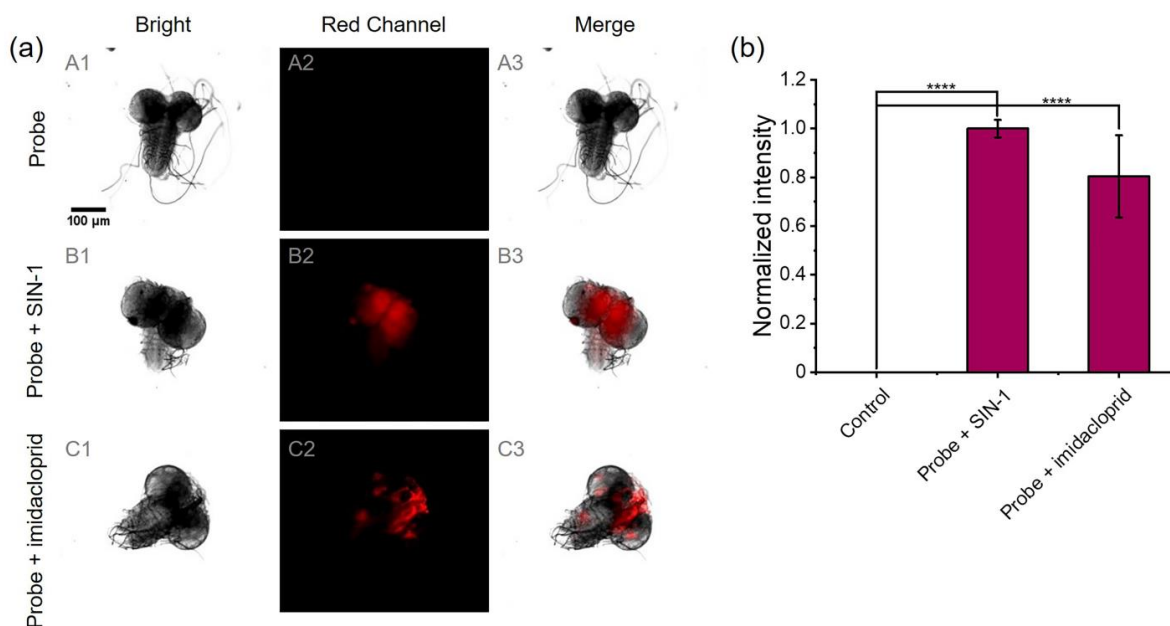


**Figure 4.** (a) Fluorescence imaging of ONOO<sup>-</sup> in *Drosophila* brains: (A1–A3) the brains incubated with NAF-BN for 30 min; (B1–B3) the brains incubated with SIN-1 (3 mM) for 4 h followed by the addition of NAF-BN for another 30 min; (C1–C3) the *Drosophila* were treated with imidacloprid (10 ppm), then the separated brains were incubated with NAF-BN for 30 min. All experiments were performed with 50 μM NAF-BN. The scale bar is 100 μm. (b) The histogram represents the mean fluorescent intensities from the corresponding images. \*\*\*\* Indicates a significant difference ( $p < 0.0001$ ) compared with the control group,  $n = 3$ .

#### 4. Conclusions

In conclusion, we have introduced **NAF-BN**, a NIR fluorescent probe capable of detecting ONOO<sup>−</sup> levels in cells and living organisms. The probe is based on a naphthalene-based fluorescein scaffold, which exhibits near-infrared fluorescence emission at 695 nm. The polycyclic-conjugated structure provides stability to the probe and the benzyl boronic acid ester moiety allows for fluorescence activation to achieve a fluorescence “off-on” response. **NAF-BN** possesses exceptional fluorescence sensitivity and good selectivity and stability for the accurate detection of ONOO<sup>−</sup> in complex physiological environments. Furthermore, our results show that **NAF-BN** is capable of detecting and imaging exogenous ONOO<sup>−</sup> from living cells, as well as in *Drosophila* brains. **NAF-BN** represents an important tool for the study and analysis of the pathophysiological functions of ONOO<sup>−</sup> in biological systems. Its excellent imaging ability make it a promising probe for future applications in the detection of ONOO<sup>−</sup> in various biological and medical research fields.

**Supplementary Materials:** The following supporting information can be downloaded at: <https://www.mdpi.com/article/10.3390/chemosensors11050286/s1>, Scheme S1: Synthetic route of **NAF-OH** and **NAF-BN**; Figure S1: Structures and properties of naphthofluoresceins; Figure S2: HRMS spectrum of **NAF-BN** (5 μM) after 15 min of reaction with ONOO<sup>−</sup> (100 μM), (a) full spectrum, (b) the spectrum of *m/z* = 400–460, (c) the spectrum of *m/z* = 810–900; Figure S3: Absorption (a) and fluorescence spectra (b) of **NAF-OH** (blue line; 5 μM) and **NAF-BN** (5 μM) after reaction with ONOO<sup>−</sup> (100 μM) for 15 min (red line) in phosphate buffer (100 mM PB, pH 7.4, with 50% DMSO). λ<sub>ex</sub> = 600 nm; slits = 5 nm/5 nm; Figure S4: Effect of different pH values on the fluorescence of **NAF-BN** (5 μM) or **NAF-BN** (5 μM) with ONOO<sup>−</sup> (100 μM) after 1 h in phosphate buffer (100 mM PB, pH 7.4, with 50% DMSO). λ<sub>ex</sub> = 600 nm, λ<sub>em</sub> = 695 nm; Figure S5: Fluorescence spectra of **NAF-OH** (5 μM) at different pH values, λ<sub>ex</sub> = 600 nm, λ<sub>em</sub> = 695 nm; Figure S6: Fluorescence response to **NAF-BN** (5 μM) with different concentrations of ONOO<sup>−</sup> for 15 min, λ<sub>ex</sub> = 600 nm, λ<sub>em</sub> = 695 nm; Figure S7: (a) Reaction of **NAF-BN** (5 μM) with ONOO<sup>−</sup> (100 μM) or H<sub>2</sub>O<sub>2</sub> (100 μM); fluorescence intensity at 695 nm versus time (0–300 s). (b) Reaction of **NAF-BN** (5 μM) with H<sub>2</sub>O<sub>2</sub> (100 μM); fluorescence intensity at 695 nm versus time (0–300 min). λ<sub>ex</sub> = 600 nm, λ<sub>em</sub> = 695 nm; Figure S8: Effect of different pH values on the fluorescence of **NAF-BN** (5 μM) after reaction with ONOO<sup>−</sup> (100 μM) or H<sub>2</sub>O<sub>2</sub> (100 μM) after 1 h in phosphate buffer (100 mM PB, pH 7.4, with 50% DMSO). λ<sub>ex</sub> = 600 nm, λ<sub>em</sub> = 695 nm; Figure S9: Fluorescence response to **NAF-BN** and different analytes for 15 min: ClO<sup>−</sup>, <sup>1</sup>O<sub>2</sub>, NO<sub>2</sub><sup>−</sup>, NO, O<sub>2</sub><sup>•−</sup>, •OH, Cys, Hcy, GSH, glucose, H<sub>2</sub>O<sub>2</sub> (1 mM); ONOO<sup>−</sup> (100 μM); and SOD (50 U/mL). All experiments were performed in phosphate buffer (100 mM PB, pH 7.4, with 50% DMSO); the concentration of **NAF-BN** was 5 μM; λ<sub>ex</sub> = 600 nm; slits = 5 nm/5 nm. (a) Acetonitrile/PB, 1/1, (b) 1,4-dioxane/PB, 1/1; Figure S10: Cell viability of 4T1 cells incubated with different concentrations of **NAF-BN**, as assessed by CCK-8 assays (incubation time 24 h); Figure S11: Cell viability of HL-7702 and 4T1 cells incubated with different concentrations of **NAF-OH**, as assessed by CCK-8 assays (incubation time 24 h); Figure S12: Cell viability of HL-7702 and 4T1 cells incubated with **NAF-BN** and SIN-1 or **NAF-BN** and PMA/LPS, as assessed by CCK-8 assays (incubation time 24 h); Figure S13: <sup>1</sup>H NMR spectrum of **NAF-OH**; Figure S14: <sup>13</sup>C NMR spectrum of **NAF-OH**; Figure S15: <sup>1</sup>H NMR spectrum of **NAF-BN**; Figure S16: <sup>13</sup>C NMR spectrum of **NAF-BN**; Figure S17: HRMS spectrum of **NAF-OH**; Figure S18: HRMS spectrum of **NAF-BN**. References [75,83–85] are cited in the supplementary materials.

**Author Contributions:** Conceptualization, W.W. and B.-O.G.; Data curation, J.-B.D.; Formal analysis, J.-B.D.; Funding acquisition, L.J. and B.-O.G.; Methodology, W.W.; Project administration, L.J. and B.-O.G.; Resources, L.J.; Supervision, W.W. and B.-O.G.; Visualization, W.W.; Writing—original draft, J.-B.D.; Writing—review and editing, W.W. and J.-B.D. All authors have read and agreed to the published version of the manuscript.

**Funding:** This work was supported by Guangdong Special Support Plan (2019TQ05X136), Guangdong Science and Technology Department (2020A0505100044, 2020A0505140005); Guangzhou Municipal Science and Technology Project (201904020032), Local Innovative and Research Teams Project of Guangdong Pearl River Talents Program (2019BT02X105), Natural Science Foundation of Guangdong Province (2019A1515012100), National Natural Science Foundation of China (62175089), and

Youth Top-notch Scientific and Technological Innovation Talent of Guangdong Special Support Plan (2019TQ05X136).

**Institutional Review Board Statement:** Not applicable.

**Informed Consent Statement:** Not applicable.

**Data Availability Statement:** Not applicable.

**Acknowledgments:** The authors thank Jie Li for technical assistance. We also thank Haiyang Xia and Yi Zhang (College of Life Science and Technology, Jinan University) for their support in cell analysis and imaging.

**Conflicts of Interest:** The authors declare no conflict of interest.

## References

1. Blough, N.V.; Zafiriou, O.C. Reaction of Superoxide with Nitric Oxide to Form Peroxonitrite in Alkaline Aqueous Solution. *Inorg. Chem.* **1985**, *24*, 3502–3504. [[CrossRef](#)]
2. Botti, H.; Moller, M.N.; Steinmann, D.; Nauser, T.; Koppenol, W.H.; Denicola, A.; Radi, R. Distance-Dependent Diffusion-Controlled Reaction of \*NO and O<sub>2</sub>\*<sup>-</sup> at Chemical Equilibrium with ONOO<sup>-</sup>. *J. Phys. Chem. B* **2010**, *114*, 16584–16593. [[CrossRef](#)]
3. Radi, R. Peroxynitrite, a Stealthy Biological Oxidant. *J. Biol. Chem.* **2013**, *288*, 26464–26472. [[CrossRef](#)]
4. Ma, Q.; Xu, S.; Zhai, Z.; Wang, K.; Liu, X.; Xiao, H.; Zhuo, S.; Liu, Y. Recent Progress of Small-Molecule Ratiometric Fluorescent Probes for Peroxynitrite in Biological Systems. *Chemistry* **2022**, *28*, e202200828. [[CrossRef](#)]
5. Ferrer-Sueta, G.; Radi, R. Chemical Biology of Peroxynitrite: Kinetics, Diffusion, and Radicals. *ACS Chem. Biol.* **2009**, *4*, 161–177. [[CrossRef](#)]
6. Lefer, A.M. Peroxynitrite as a Cytoprotective Agent in Myocardial Ischemia/Reperfusion Injury. *Pathophysiology* **1998**, *5*, 38. [[CrossRef](#)]
7. Sies, H.; Jones, D.P. Reactive Oxygen Species (ROS) as Pleiotropic Physiological Signalling Agents. *Nat. Rev. Mol. Cell Biol.* **2020**, *21*, 363–383. [[CrossRef](#)]
8. Vana, L.; Kanaan, N.M.; Hakala, K.; Weintraub, S.T.; Binder, L.I. Peroxynitrite-Induced Nitratative and Oxidative Modifications Alter Tau Filament Formation. *Biochemistry* **2011**, *50*, 1203–1212. [[CrossRef](#)]
9. Szabo, C. Multiple Pathways of Peroxynitrite Cytotoxicity. *Toxicol. Lett.* **2003**, *140–141*, 105–112. [[CrossRef](#)]
10. Szabo, C. DNA Strand Breakage and Activation of Poly-Adp Ribosyltransferase: A Cytotoxic Pathway Triggered by Peroxynitrite. *Free Radic. Biol. Med.* **1996**, *21*, 855–869. [[CrossRef](#)]
11. Pandey, V.K.; Amin, P.J.; Shankar, B.S. G1-4a, a Polysaccharide from *Tinospora Cordifolia* Induces Peroxynitrite Dependent Killer Dendritic Cell (KDC) Activity against Tumor Cells. *Int. Immunopharmacol.* **2014**, *23*, 480–488. [[CrossRef](#)] [[PubMed](#)]
12. Xia, H.; Zhang, L.; Dai, J.; Liu, X.; Zhang, X.; Zeng, Z.; Jia, Y. Effect of Selenium and Peroxynitrite on Immune Function of Immature Dendritic Cells in Humans. *Med. Sci. Monit* **2021**, *27*, e929004. [[CrossRef](#)] [[PubMed](#)]
13. Greten, F.R.; Grivnennikov, S.I. Inflammation and Cancer: Triggers, Mechanisms, and Consequences. *Immunity* **2019**, *51*, 27–41. [[CrossRef](#)]
14. Salvemini, D.; Doyle, T.M.; Cuzzocrea, S. Superoxide, Peroxynitrite and Oxidative/Nitratative Stress in Inflammation. *Biochem. Soc. Trans.* **2006**, *34*, 965–970. [[CrossRef](#)] [[PubMed](#)]
15. Dedon, P.C.; Tannenbaum, S.R. Reactive Nitrogen Species in the Chemical Biology of Inflammation. *Arch Biochem. Biophys.* **2004**, *423*, 12–22. [[CrossRef](#)]
16. Cobb, C.A.; Cole, M.P. Oxidative and Nitratative Stress in Neurodegeneration. *Neurobiol. Dis.* **2015**, *84*, 4–21. [[CrossRef](#)]
17. Barnham, K.J.; Masters, C.L.; Bush, A.I. Neurodegenerative Diseases and Oxidative Stress. *Nat. Rev. Drug Discov.* **2004**, *3*, 205–214. [[CrossRef](#)]
18. Li, J.; Su, J.; Li, W.; Liu, W.; Altura, B.T.; Altura, B.M. Peroxynitrite Induces Apoptosis in Canine Cerebral Vascular Muscle Cells: Possible Relation to Neurodegenerative Diseases and Strokes. *Neurosci. Lett.* **2003**, *350*, 173–177. [[CrossRef](#)]
19. Mungrue, I.N.; Gros, R.; You, X.; Pirani, A.; Azad, A.; Csont, T.; Schulz, R.; Butany, J.; Stewart, D.J.; Husain, M. Cardiomyocyte Overexpression of Inos in Mice Results in Peroxynitrite Generation, Heart Block, and Sudden Death. *J. Clin. Investig.* **2002**, *109*, 735–743. [[CrossRef](#)]
20. van der Loo, B.; Labugger, R.; Skepper, J.N.; Bachschmid, M.; Kilo, J.; Powell, J.M.; Palacios-Callender, M.; Erusalimsky, J.D.; Quaschnig, T.; Malinski, T.; et al. Enhanced Peroxynitrite Formation Is Associated with Vascular Aging. *J. Exp. Med.* **2000**, *192*, 1731–1744. [[CrossRef](#)]
21. Shuhendler, A.J.; Pu, K.; Cui, L.; Uetrecht, J.P.; Rao, J. Real-Time Imaging of Oxidative and Nitrosative Stress in the Liver of Live Animals for Drug-Toxicity Testing. *Nat. Biotechnol.* **2014**, *32*, 373–380. [[CrossRef](#)] [[PubMed](#)]
22. Peng, J.; Samanta, A.; Zeng, X.; Han, S.; Wang, L.; Su, D.; Loong, D.T.; Kang, N.Y.; Park, S.J.; All, A.H.; et al. Real-Time in vivo Hepatotoxicity Monitoring through Chromophore-Conjugated Photon-Upconverting Nanoprobes. *Angew. Chem. Int. Ed. Engl.* **2017**, *56*, 4165–4169. [[CrossRef](#)] [[PubMed](#)]

23. Graham, P.M.; Li, J.Z.; Dou, X.; Zhu, H.; Misra, H.P.; Jia, Z.; Li, Y. Protection against Peroxynitrite-Induced DNA Damage by Mesalamine: Implications for Anti-Inflammation and Anti-Cancer Activity. *Mol. Cell Biochem.* **2013**, *378*, 291–298. [[CrossRef](#)] [[PubMed](#)]
24. Vasilescu, A.; Gheorghiu, M.; Petcu, S. Nanomaterial-Based Electrochemical Sensors and Optical Probes for Detection and Imaging of Peroxynitrite: A Review. *Microchim. Acta* **2017**, *184*, 649–675. [[CrossRef](#)]
25. Hulvey, M.K.; Frankenfeld, C.N.; Lunte, S.M. Separation and Detection of Peroxynitrite Using Microchip Electrophoresis with Amperometric Detection. *Anal. Chem.* **2010**, *82*, 1608–1611. [[CrossRef](#)]
26. Eliasson, M.J.; Huang, Z.; Ferrante, R.J.; Sasamata, M.; Molliver, M.E.; Snyder, S.H.; Moskowitz, M.A. Neuronal Nitric Oxide Synthase Activation and Peroxynitrite Formation in Ischemic Stroke Linked to Neural Damage. *J. Neurosci.* **1999**, *19*, 5910–5918. [[CrossRef](#)]
27. Imaram, W.; Gersch, C.; Kim, K.M.; Johnson, R.J.; Henderson, G.N.; Angerhofer, A. Radicals in the Reaction between Peroxynitrite and Uric Acid Identified by Electron Spin Resonance Spectroscopy and Liquid Chromatography Mass Spectrometry. *Free Radic. Biol. Med.* **2010**, *49*, 275–281. [[CrossRef](#)]
28. Jiao, X.; Li, Y.; Niu, J.; Xie, X.; Wang, X.; Tang, B. Small-Molecule Fluorescent Probes for Imaging and Detection of Reactive Oxygen, Nitrogen, and Sulfur Species in Biological Systems. *Anal. Chem.* **2018**, *90*, 533–555. [[CrossRef](#)]
29. Cui, W.L.; Wang, M.H.; Yang, Y.H.; Wang, J.Y.; Zhu, X.Z.; Zhang, H.T.; Ji, X.X. Recent Advances and Perspectives in Reaction-Based Fluorescent Probes for Imaging Peroxynitrite in Biological Systems. *Coord. Chem. Rev.* **2023**, *474*, 214848. [[CrossRef](#)]
30. Sedgwick, A.C.; Dou, W.T.; Jiao, J.B.; Wu, L.; Williams, G.T.; Jenkins, A.T.A.; Bull, S.D.; Sessler, J.L.; He, X.P.; James, T.D. An Esipt Probe for the Ratiometric Imaging of Peroxynitrite Facilitated by Binding to Abeta-Aggregates. *J. Am. Chem. Soc.* **2018**, *140*, 14267–14271. [[CrossRef](#)]
31. Wu, L.; Wang, Y.; Weber, M.; Liu, L.; Sedgwick, A.C.; Bull, S.D.; Huang, C.; James, T.D. Esipt-Based Ratiometric Fluorescence Probe for the Intracellular Imaging of Peroxynitrite. *Chem. Commun.* **2018**, *54*, 9953–9956. [[CrossRef](#)] [[PubMed](#)]
32. Shu, W.; Wu, Y.L.; Zang, S.P.; Su, S.; Kang, H.; Jing, J.; Zhang, X.L. A Mitochondria-Targeting Highly Specific Fluorescent Probe for Fast Sensing of Endogenous Peroxynitrite in Living Cells. *Sens. Actuators B Chem.* **2020**, *303*, 127284. [[CrossRef](#)]
33. Xia, L.; Tong, Y.; Li, L.; Cui, M.; Gu, Y.; Wang, P. A Selective Fluorescent Turn-on Probe for Imaging Peroxynitrite in Living Cells and Drug-Damaged Liver Tissues. *Talanta* **2019**, *204*, 431–437. [[CrossRef](#)] [[PubMed](#)]
34. Odyniec, M.L.; Park, S.J.; Gardiner, J.E.; Webb, E.C.; Sedgwick, A.C.; Yoon, J.; Bull, S.D.; Kim, H.M.; James, T.D. A Fluorescent Esipt-Based Benzimidazole Platform for the Ratiometric Two-Photon Imaging of ONOO<sup>-</sup> in vitro and ex vivo. *Chem. Sci.* **2020**, *11*, 7329–7334. [[CrossRef](#)] [[PubMed](#)]
35. Qu, W.; Niu, C.; Zhang, X.; Chen, W.; Yu, F.; Liu, H.; Zhang, X.; Wang, S. Construction of a Novel Far-Red Fluorescence Light-up Probe for Visualizing Intracellular Peroxynitrite. *Talanta* **2019**, *197*, 431–435. [[CrossRef](#)]
36. Li, Y.; Wu, Y.; Chen, L.; Zeng, H.; Chen, X.; Lun, W.; Fan, X.; Wong, W.Y. A Time-Resolved near-Infrared Phosphorescent Iridium(III) Complex for Fast and Highly Specific Peroxynitrite Detection and Bioimaging Applications. *J. Mater. Chem. B* **2019**, *7*, 7612–7618. [[CrossRef](#)]
37. Zhang, K.; Wang, Z.; Hu, X.; Meng, J.; Bao, W.; Wang, X.; Ding, W.; Tian, Z. A Long-Wavelength Turn-on Fluorescent Probe for Intracellular Nanomolar Level Peroxynitrite Sensing with Second-Level Response. *Talanta* **2020**, *219*, 121354. [[CrossRef](#)]
38. Zhou, Y.; Li, P.; Fan, N.; Wang, X.; Liu, X.; Wu, L.; Zhang, W.; Zhang, W.; Ma, C.; Tang, B. In Situ Visualization of Peroxisomal Peroxynitrite in the Livers of Mice with Acute Liver Injury Induced by Carbon Tetrachloride Using a New Two-Photon Fluorescent Probe. *Chem. Commun.* **2019**, *55*, 6767–6770. [[CrossRef](#)]
39. Yan, M.; Fang, H.X.; Wang, X.Q.; Xu, J.J.; Zhang, C.W.; Xu, L.; Li, L. A Two-Photon Fluorescent Probe for Visualizing Endoplasmic Reticulum Peroxynitrite in Parkinson's Disease Models. *Sens. Actuators B Chem.* **2021**, *328*, 129003. [[CrossRef](#)]
40. Liu, X.; Gu, F.; Zhou, X.; Zhou, W.; Zhang, S.; Cui, L.; Guo, T. A Naphthalimide-Based Turn-on Fluorescence Probe for Peroxynitrite Detection and Imaging in Living Cells. *RSC Adv.* **2020**, *10*, 38281–38286. [[CrossRef](#)]
41. Li, M.; Gong, X.; Li, H.W.; Han, H.; Shuang, S.; Song, S.; Dong, C. A Fast Detection of Peroxynitrite in Living Cells. *Anal. Chim. Acta* **2020**, *1106*, 96–102. [[CrossRef](#)] [[PubMed](#)]
42. Zhu, B.C.; Zhang, M.; Wu, L.; Zhao, Z.Y.; Liu, C.Y.; Wang, Z.K.; Duan, Q.X.; Wang, Y.W.; Jia, P. A Highly Specific Far-Red Fluorescent Probe for Imaging Endogenous Peroxynitrite in the Mitochondria of Living Cells. *Sens. Actuators B Chem.* **2018**, *257*, 436–441. [[CrossRef](#)]
43. Guria, U.N.; Gangopadhyay, A.; Ali, S.S.; Maiti, K.; Samanta, S.K.; Manna, S.; Ghosh, A.K.; Uddin, M.R.; Mandal, S.; Mahapatra, A.K. A Benzothiazole-Conjugated Hemicyanine Dye as a Ratiometric NIR Fluorescent Probe for the Detection and Imaging of Peroxynitrite in Living Cells. *Anal. Methods* **2019**, *11*, 5447–5454. [[CrossRef](#)]
44. Fang, Y.; Chen, R.-X.; Qin, H.-F.; Wang, J.-J.; Zhang, Q.; Chen, S.; Wen, Y.-H.; Wang, K.-P.; Hu, Z.-Q. A Chromene Based Fluorescence Probe: Accurate Detection of Peroxynitrite in Mitochondria, Not Elsewhere. *Sens. Actuators B Chem.* **2021**, *334*, 129603. [[CrossRef](#)]
45. Yuan, R.Q.; Ma, Y.H.; Du, J.Y.; Meng, F.X.; Guo, J.J.; Hong, M.; Yue, Q.L.; Li, X.; Li, C.Z. A Novel Highly Selective near-Infrared and Naked-Eye Fluorescence Probe for Imaging Peroxynitrite. *Anal. Methods* **2019**, *11*, 1522–1529. [[CrossRef](#)]
46. Wu, Y.; Shi, A.; Li, Y.; Zeng, H.; Chen, X.; Wu, J.; Fan, X. A near-Infrared Xanthene Fluorescence Probe for Monitoring Peroxynitrite in Living Cells and Mouse Inflammation Model. *Analyst* **2018**, *143*, 5512–5519. [[CrossRef](#)]

47. Zhou, D.Y.; Juan, O.Y.; Li, Y.; Jiang, W.L.; Yang, T.; Yi, Z.M.; Li, C.Y. A Ratiometric Fluorescent Probe for the Detection of Peroxynitrite with Simple Synthesis and Large Emission Shift and Its Application in Cells Image. *Dye. Pigment.* **2019**, *161*, 288–295. [[CrossRef](#)]
48. Zhang, J.; Kan, J.; Sun, Y.; Won, M.; Kim, J.H.; Zhang, W.; Zhou, J.; Qian, Z.; Kim, J.S. Nanoliposomal Ratiometric Fluorescent Probe toward ONOO(−) Flux. *ACS Appl. Bio. Mater.* **2021**, *4*, 2080–2088. [[CrossRef](#)]
49. An, Q.; Su, S.Z.; Chai, L.; Wang, Y.Y.; Wang, X.M.; Li, X.C.; Liang, T.; Hu, W.; Song, X.J.; Li, C.Y. Imaging of Peroxynitrite in Mitochondria by a near-Infrared Fluorescent Probe with a Large Stokes Shift. *Talanta* **2023**, *253*, 124073. [[CrossRef](#)]
50. Yu, F.; Li, P.; Wang, B.; Han, K. Reversible Near-Infrared Fluorescent Probe Introducing Tellurium to Mimetic Glutathione Peroxidase for Monitoring the Redox Cycles between Peroxynitrite and Glutathione in vivo. *J. Am. Chem. Soc.* **2013**, *135*, 7674–7680. [[CrossRef](#)]
51. Yu, F.; Li, P.; Li, G.; Zhao, G.; Chu, T.; Han, K. A near-Ir Reversible Fluorescent Probe Modulated by Selenium for Monitoring Peroxynitrite and Imaging in Living Cells. *J. Am. Chem. Soc.* **2011**, *133*, 11030–11033. [[CrossRef](#)] [[PubMed](#)]
52. Hou, T.; Zhang, K.; Kang, X.; Guo, X.; Du, L.; Chen, X.; Yu, L.; Yue, J.; Ge, H.; Liu, Y.; et al. Sensitive Detection and Imaging of Endogenous Peroxynitrite Using a Benzo[D]Thiazole Derived Cyanine Probe. *Talanta* **2019**, *196*, 345–351. [[CrossRef](#)] [[PubMed](#)]
53. Zhang, W.; Liu, Y.; Gao, Q.; Liu, C.; Song, B.; Zhang, R.; Yuan, J. A Ruthenium(Ii) Complex-Cyanine Energy Transfer Scaffold Based Luminescence Probe for Ratiometric Detection and Imaging of Mitochondrial Peroxynitrite. *Chem. Commun.* **2018**, *54*, 13698–13701. [[CrossRef](#)]
54. Xue, X.L.; Zhang, H.; Chen, G.H.; Yu, G.H.; Hu, H.R.; Niu, S.Y.; Wang, K.P.; Hu, Z.Q. Coumarin-Cyanine Hybrid: A Ratiometric Fluorescent Probe for Accurate Detection of Peroxynitrite in Mitochondria. *Spectrochim. Acta A Mol. Biomol. Spectrosc.* **2023**, *292*, 122443. [[CrossRef](#)]
55. Johnson, R.E.; van der Zalm, J.M.; Chen, A.; Bell, I.J.; Van Raay, T.J.; Al-Abdul-Wahid, M.S.; Manderville, R.A. Unraveling the Chemosensing Mechanism by the 7-(Diethylamino) Coumarin-Hemicyanine Hybrid: A Ratiometric Fluorescent Probe for Hydrogen Peroxide. *Anal. Chem.* **2022**, *94*, 11047–11054. [[CrossRef](#)] [[PubMed](#)]
56. Bolland, H.R.; Hammond, E.M.; Sedgwick, A.C. A Fluorescent Probe Strategy for the Detection and Discrimination of Hydrogen Peroxide and Peroxynitrite in Cells. *Chem. Commun.* **2022**, *58*, 10699–10702. [[CrossRef](#)] [[PubMed](#)]
57. Albers, A.E.; Dickinson, B.C.; Miller, E.W.; Chang, C.J. A Red-Emitting Naphthofluorescein-Based Fluorescent Probe for Selective Detection of Hydrogen Peroxide in Living Cells. *Bioorg. Med. Chem. Lett.* **2008**, *18*, 5948–5950. [[CrossRef](#)]
58. Hou, J.; Qian, M.; Zhao, H.; Li, Y.; Liao, Y.; Han, G.; Xu, Z.; Wang, F.; Song, Y.; Liu, Y. A near-Infrared Ratiometric/Turn-on Fluorescent Probe for in vivo Imaging of Hydrogen Peroxide in a Murine Model of Acute Inflammation. *Anal. Chim. Acta* **2018**, *1024*, 169–176. [[CrossRef](#)]
59. Wang, K.; Ma, W.; Xu, Y.; Liu, X.; Chen, G.; Yu, M.; Pan, Q.; Huang, C.; Li, X.; Mu, Q.; et al. Design of a Novel Mitochondria Targetable Turn-on Fluorescence Probe for Hydrogen Peroxide and Its Two-Photon Bioimaging Applications. *Chin. Chem. Lett.* **2020**, *31*, 3149–3152. [[CrossRef](#)]
60. Wang, W.X.; Jiang, W.L.; Mao, G.J.; Tan, M.; Fei, J.; Li, Y.; Li, C.Y. Monitoring the Fluctuation of Hydrogen Peroxide in Diabetes and Its Complications with a Novel Near-Infrared Fluorescent Probe. *Anal. Chem.* **2021**, *93*, 3301–3307. [[CrossRef](#)]
61. Sikora, A.; Zielonka, J.; Lopez, M.; Joseph, J.; Kalyanaraman, B. Direct Oxidation of Boronates by Peroxynitrite: Mechanism and Implications in Fluorescence Imaging of Peroxynitrite. *Free Radic. Biol. Med.* **2009**, *47*, 1401–1407. [[CrossRef](#)]
62. Jourden, J.L.; Daniel, K.B.; Cohen, S.M. Investigation of Self-Immolative Linkers in the Design of Hydrogen Peroxide Activated Metalloprotein Inhibitors. *Chem. Commun.* **2011**, *47*, 7968–7970. [[CrossRef](#)] [[PubMed](#)]
63. Daniel, K.B.; Agrawal, A.; Manchester, M.; Cohen, S.M. Readily Accessible Fluorescent Probes for Sensitive Biological Imaging of Hydrogen Peroxide. *Chembiochem* **2013**, *14*, 593–598. [[CrossRef](#)] [[PubMed](#)]
64. Zielonka, J.; Sikora, A.; Hardy, M.; Joseph, J.; Dranka, B.P.; Kalyanaraman, B. Boronate Probes as Diagnostic Tools for Real Time Monitoring of Peroxynitrite and Hydroperoxides. *Chem. Res. Toxicol.* **2012**, *25*, 1793–1799. [[CrossRef](#)] [[PubMed](#)]
65. Martin-Romero, F.J.; Gutierrez-Martin, Y.; Henao, F.; Gutierrez-Merino, C. Fluorescence Measurements of Steady State Peroxynitrite Production Upon Sin-1 Decomposition: Nadh Versus Dihydrodichlorofluorescein and Dihydrorhodamine 123. *J. Fluoresc.* **2004**, *14*, 17–23. [[CrossRef](#)] [[PubMed](#)]
66. Dai, C.; Ciccotosto, G.D.; Cappai, R.; Wang, Y.; Tang, S.; Xiao, X.; Velkov, T. Minocycline Attenuates Colistin-Induced Neurotoxicity via Suppression of Apoptosis, Mitochondrial Dysfunction and Oxidative Stress. *J. Antimicrob. Chemother.* **2017**, *72*, 1635–1645. [[CrossRef](#)]
67. Tyagi, S.R.; Tamura, M.; Burnham, D.N.; Lambeth, J.D. Phorbol Myristate Acetate (PMA) Augments Chemoattractant-Induced Diglyceride Generation in Human Neutrophils but Inhibits Phosphoinositide Hydrolysis. Implications for the Mechanism of PMA Priming of the Respiratory Burst. *J. Biol. Chem.* **1988**, *263*, 13191–13198. [[CrossRef](#)]
68. Chung, T.H.; Wu, Y.P.; Chew, C.Y.; Lam, C.H.; Tan, K.T. Imaging and Quantification of Secreted Peroxynitrite at the Cell Surface by a Streptavidin-Biotin-Controlled Binding Probe. *Chembiochem* **2018**, *19*, 2584–2590. [[CrossRef](#)]
69. Deng, Y.; Feng, G. Visualization of ONOO<sup>−</sup> and Viscosity in Drug-Induced Hepatotoxicity with Different Fluorescence Signals by a Sensitive Fluorescent Probe. *Anal. Chem.* **2020**, *92*, 14667–14675. [[CrossRef](#)]
70. Lu, J.; Li, Z.; Zheng, X.; Tan, J.; Ji, Z.; Sun, Z.; You, J. A Rapid Response near-Infrared Ratiometric Fluorescent Probe for the Real-Time Tracking of Peroxynitrite for Pathological Diagnosis and Therapeutic Assessment in a Rheumatoid Arthritis Model. *J. Mater. Chem. B* **2020**, *8*, 9343–9350. [[CrossRef](#)]

71. Wang, P.; Yu, L.; Gong, J.; Xiong, J.; Zi, S.; Xie, H.; Zhang, F.; Mao, Z.; Liu, Z.; Kim, J.S. An Activity-Based Fluorescent Probe for Imaging Fluctuations of Peroxynitrite (ONOO<sup>-</sup>) in the Alzheimer's Disease Brain. *Angew. Chem. Int. Ed. Engl.* **2022**, *61*, e202206894. [[CrossRef](#)] [[PubMed](#)]
72. Mao, G.J.; Gao, G.Q.; Dong, W.P.; Wang, Q.Q.; Wang, Y.Y.; Li, Y.; Su, L.; Zhang, G. A Two-Photon Excited near-Infrared Fluorescent Probe for Imaging Peroxynitrite during Drug-Induced Hepatotoxicity and Its Remediation. *Talanta* **2021**, *221*, 121607. [[CrossRef](#)] [[PubMed](#)]
73. Xin, F.; Zhao, J.; Shu, W.; Zhang, X.; Luo, X.; Tian, Y.; Xing, M.; Wang, H.; Peng, Y.; Tian, Y. A Thiocarbonate-Caged Fluorescent Probe for Specific Visualization of Peroxynitrite in Living Cells and Zebrafish. *Analyst* **2021**, *146*, 7627–7634. [[CrossRef](#)] [[PubMed](#)]
74. Liu, Y.; Ma, Y.; Lin, W. Construction of a Bi-Functional Ratiometric Fluorescent Probe for Detection of Endoplasmic Reticulum Viscosity and ONOO<sup>-</sup> in Cells and Zebrafish. *Sens. Actuators B Chem.* **2022**, *373*, 132742. [[CrossRef](#)]
75. Sun, Q.; Xu, J.; Ji, C.; Shaibani, M.S.S.; Li, Z.; Lim, K.; Zhang, C.; Li, L.; Liu, Z. Ultrafast Detection of Peroxynitrite in Parkinson's Disease Models Using a near-Infrared Fluorescent Probe. *Anal. Chem.* **2020**, *92*, 4038–4045. [[CrossRef](#)]
76. Azuma, E.; Nakamura, N.; Kuramochi, K.; Sasamori, T.; Tokitoh, N.; Sagami, I.; Tsubaki, K. Exhaustive Syntheses of Naphthofluoresceins and Their Functions. *J. Org. Chem.* **2012**, *77*, 3492–3500. [[CrossRef](#)]
77. Lee, L.G.; Berry, G.M.; Chen, C.H. Vita Blue: A New 633-Nm Excitable Fluorescent Dye for Cell Analysis. *Cytometry* **1989**, *10*, 151–164. [[CrossRef](#)]
78. Salerno, M.; Ajimo, J.J.; Dudley, J.A.; Binzel, K.; Urayama, P. Characterization of Dual-Wavelength Seminaphthofluorescein and Seminaphthorhodafluor Dyes for Ph Sensing under High Hydrostatic Pressures. *Anal. Biochem.* **2007**, *362*, 258–267. [[CrossRef](#)]
79. Yamaguchi, M.; Yoshida, H. *Drosophila as a Model Organism*. In *Drosophila Models for Human Diseases*; Yamaguchi, M., Ed.; Springer: Singapore, 2018; pp. 1–10.
80. Yucel, M.S.; Kayis, T. Imidacloprid Induced Alterations in Oxidative Stress, Biochemical, Genotoxic, and Immunotoxic Biomarkers in Non-Mammalian Model Organism *Galleria mellonella* L. (Lepidoptera: Pyralidae). *J. Environ. Sci. Health B* **2019**, *54*, 27–34. [[CrossRef](#)]
81. Li, Z.; Yu, T.; Chen, Y.; Heerman, M.; He, J.; Huang, J.; Nie, H.; Su, S. Brain Transcriptome of Honey Bees (*Apis mellifera*) Exhibiting Impaired Olfactory Learning Induced by a Sublethal Dose of Imidacloprid. *Pestic. Biochem. Physiol.* **2019**, *156*, 36–43. [[CrossRef](#)]
82. Martelli, F.; Zhongyuan, Z.; Wang, J.; Wong, C.O.; Karagas, N.E.; Roessner, U.; Rupasinghe, T.; Venkatachalam, K.; Perry, T.; Bellen, H.J.; et al. Low Doses of the Neonicotinoid Insecticide Imidacloprid Induce ROS Triggering Neurological and Metabolic Impairments in *Drosophila*. *Proc. Natl. Acad. Sci. USA* **2020**, *117*, 25840–25850. [[CrossRef](#)] [[PubMed](#)]
83. Li, H.; Shi, W.; Li, X.; Hu, Y.; Fang, Y.; Ma, H. Ferroptosis Accompanied by •OH Generation and Cytoplasmic Viscosity Increase Revealed Via Dual-Functional Fluorescence Probe. *J Am Chem Soc* **2019**, *141*, 18301–18307. [[CrossRef](#)] [[PubMed](#)]
84. Massey, V.; Komai, H.; Palmer, G.; Elion, G.B. On the Mechanism of Inactivation of Xanthine Oxidase by Allopurinol and Other Pyrazolo[3,4-D]Pyrimidines. *J. Biol. Chem.* **1970**, *245*, 2837–2844. [[CrossRef](#)] [[PubMed](#)]
85. Suo, F.T.; Chen, X.W.; Fang, H.X.; Gong, Q.Y.; Yu, C.M.; Yang, N.D.; Li, S.; Wu, Q.; Li, L.; Huang, W. Hybrid Fluorophores-Based Fluorogenic Paper Device for Visually High-Throughput Detection of Cu<sup>2+</sup> in Real Samples. *Dyes Pigm.* **2019**, *170*, 107639. [[CrossRef](#)]

**Disclaimer/Publisher's Note:** The statements, opinions and data contained in all publications are solely those of the individual author(s) and contributor(s) and not of MDPI and/or the editor(s). MDPI and/or the editor(s) disclaim responsibility for any injury to people or property resulting from any ideas, methods, instructions or products referred to in the content.